# Unitary model analysis of $f_0(500)$ pole positions by continuously varying $m_\pi$: Comparison with discrete lattice predictions

George Rupp
*Center for Theoretical Particle Physics, Instituto Superior Técnico,*
*Universidade de Lisboa, P-1049-001 Lisboa, Portugal*

Resonance, bound-state, and virtual-state pole positions of the $f_0(500)$ scalar meson are computed as a continuous function of pion mass in the framework of a unitarized and analytic coupled-channel model for scalar mesons, described as dynamical quark-antiquark states. The $f_0(500)$ is modeled with both light and strange $q\bar{q}$ seeds, mixing with each other through the common $S$-wave $\pi\pi$, $K\bar{K}$, and $\eta\eta$ meson-meson decay channels. The few model parameters are fitted to experimental $S$-wave $\pi\pi$ phase shifts up to 1 GeV. In the case of the physical $\pi^\pm$ mass of 139.57 MeV, resonance poles at $(460 - i222)$ MeV and $(978 - i37.2)$ MeV are found for the $f_0(500)$ and $f_0(980)$, respectively. Resonance, bound-state, and virtual-state pole trajectories are computed and plotted as a function of pion masses up to 500 MeV, both in the complex-energy and complex-momentum planes. The results are discussed and compared to the most advanced lattice QCD computations employing interpolators that correspond to the $q\bar{q}$ and meson-meson channels in the present model, that is, for a few discrete values of the unphysical pion mass in those lattice calculations.

## I. INTRODUCTION

The light scalar mesons $f_0(500)$ (alias $\sigma$), $f_0(980)$, $K_0^\star(700)$ (alias $\kappa$), and $a_0(980)$ [1] have long eluded experimentalists as well as theorists (see Ref. [2] for a minireview). On the one hand, the very existence of especially the extremely broad $\sigma$ and $\kappa$ as genuine mesons has for many years been questioned, due to the difficulty to identify unmistakable resonance signals in scattering and production experiments. On the other hand, all four scalars have been highly problematic to understand in the context of conventional quark models, in view of their seemingly much too low masses as $P$-wave quark-antiquark states. A very original and relatively successful solution was proposed by R. L. Jaffe [3] in 1977, suggesting that the above four scalars are $qq\bar{q}\bar{q}$ (tetraquark) states rather than regular $q\bar{q}$ mesons. Owing to a very large and attractive color-spin interaction for the ground-state $S$-wave tetraquarks, their masses come out several hundreds of MeV below the typical mass range of 1.3–1.5 GeV for $P$-wave mesons, thus allowing to predict much more reasonable masses, albeit still somewhat on the high side [1,3]. Nevertheless, Jaffe himself admitted [3,4] that mass calculations of

mesons whose very large widths are ignored must not be taken too literally and an accuracy as usually obtained for regular hadrons should not be expected. He also observed [3,4] that such $q^2\bar{q}^2$ systems can just fall apart into two light mesons, not requiring the creation of a new $q\bar{q}$ pair like in the case of normal mesons, thus being processes of order $N_c^0$ instead of $N_c^{-1}$.

However, a few years later, my co-authors and I found [5,6] a $\sigma$-meson resonance pole in the correct mass ballpark and with a realistic width, in the framework of a unitarized coupled-channel model [7] for confined $q\bar{q}$ systems interacting with two-meson states. This "unquenched" quark model had just been developed to describe both light and heavy vector as well as pseudoscalar mesons by including the nonperturbative dynamical effects of strong decay. This $\sigma$ pole turned out to be of a dynamical origin, i.e., arising from the $\pi\pi$ scattering continuum for increasing decay strength and not directly linked to an intrinsic quark-model state. An equally dynamical $f_0(980)$ pole appeared as well, just like the $\sigma(500)$ with a reasonable mass and width, besides regular $f_0(1370)$ and $f_0(1500)$ [1] scalar resonance poles predicted in mainstream quark models. Moreover, the gross behavior of the $S$-wave $\pi\pi$ scattering phase shifts was also automatically reproduced [5]. In Ref. [8], this model calculation was extended to the other light scalars as well, resulting in predicted resonance pole positions for the $\sigma$, $\kappa$, $f_0(980)$, and $a_0(980)$ that are still within current PDG limits [1], using the very same parameter values as those found in the fit carried out in Ref. [7].

When the four light scalars had finally been confirmed experimentally and lattice QCD (LQCD) had made sufficient progress so as to be capable of carrying out some reliable simulations of meson resonances, first results on the light scalars started to appear in the literature (see the review paper Ref. [9]). In particular, in Ref. [10] an LQCD computation of isoscalar $S$-wave $\pi\pi$ phase shifts was done for the two unphysical pion masses of 391 MeV and 236 MeV, while searching for bound states and/or resonance poles. The simulation employed single-meson $u\bar{u} + d\bar{d}$ and $s\bar{s}$ interpolating fields as well as $\pi\pi$ and $K\bar{K}$ two-meson interpolators. As a result, a $\pi\pi$ bound state was found at 758(4) MeV for the heavier pion mass, whereas $\sigma$-like resonance pole positions were extracted for the lighter pion, using a variety of parametrizations, albeit widely spread out in energy and with large to very large error bars. A year later, a more extensive and detailed lattice analysis [11] was published, namely of not only the light scalars, but also the lowest isoscalar tensor mesons $f_2(1270)$ and $f_2'(1525)$. In the case of the $\sigma$ and $f_0(980)$, an $\eta\eta$ interpolating field was included as well. In this simulation, only $m_\pi = 391$ MeV was considered, resulting in a $\sigma$-type bound state slightly lighter than in Ref. [10], viz. at 745(5) MeV.

In the present paper, I will present a unitarized coupled-channel model for the $\sigma$ resonance, in the spirit of Ref. [8] yet formulated in momentum space following the resonance spectrum expansion (RSE) [12,13]. The goal is to study in detail the behavior of the $\sigma$ pole, not only for the two unphysical pion masses of 391 MeV [10,11] and 236 MeV [10], but rather as a continuous function of $m_\pi$ over a wide range of values starting at the pion's physical mass. As the model is manifestly unitary and analytic, it may shed some light on aspects of the parametrizations employed in Refs. [10,11]. Since after I concluded the present study my attention was drawn to two very recent LQCD papers involving authors of Refs. [10,11] that present results for two intermediate pion masses [14] and extracted $\sigma$ pole positions further restricted by dispersive methods [15], I shall briefly discuss these papers below as well.

Another purpose of the present paper is to see how precisely the $\sigma$ resonance pole for varying $m_\pi$ is connected not only to a bound state but also to possible virtual states. This will furthermore serve to explicitly check a claim made in the dispersive analysis of Ref. [16] about a virtual $\sigma$ pole not far from the bound-state pole at 758(4) as found in

Ref. [10] for $m_\pi = 391$ MeV. A comment on this claim was already published in Ref. [17], in the context of a model [18] very similar to the present one, but vaster in scope so as to also investigate the $f_0(980)$ and $a_0(980)$, as well as the standard quark-model scalar mesons $f_0(1370)$ and $a_0(1450)$.

This paper is organized as follows. In Sec. II the here employed RSE model will be described in detail, including a closed-form expression for the multichannel $S$-matrix, and a fit to $S$-wave $\pi\pi$ phase shifts will be carried out. In Sec. III, I will present several figures of the resulting $\sigma$ resonance, bound-state, and virtual-state trajectories as a continuous function of pion mass. Finally, Sec. IV will be devoted to some discussion and conclusions in connection with the mentioned LQCD results.

## II. RSE MODEL FOR AN ISOSCALAR SCALAR

The RSE model for nonexotic meson spectroscopy is based on an $s$-channel propagator of a bare meson and its excitations, which couple in the intermediate state to an incoming pair of mesons and then to an outgoing meson pair that may be different from the incoming one. Note that this model is not suited to describe meson-meson (MM) scattering for quantum numbers not supported by $q\bar{q}$ states, as e.g. $I = 2$. Also, crossing-symmetry constraints are not explicitly imposed. However, it has been argued by different authors that nonexotic meson resonances are dominated by several $s$-channel exchanges, which according to duality also account for some $t$- and $u$-channel phenomena (see Ref. [17] for references). The RSE bubble sum for the $\pi\pi \to \pi\pi$ $T$-matrix element is depicted in Fig. 1, where we take towers of bare $n\bar{n} \equiv (u\bar{u} + d\bar{d})/\sqrt{2}$ and $s\bar{s}$ states coupling to the asymptotic two-meson channels $\pi\pi$, $K\bar{K}$, and $\eta\eta$. The Born term in the figure stands for two incoming pions, which at the initial vertex couple to intermediate $n\bar{n}$ and $s\bar{s}$ states with all their excitations—represented by the wiggly line—via one $q\bar{q}$ annihilation. After propagation of these states, a new $q\bar{q}$ pair is created at the second vertex, giving rise to two pions again in the final state. Note that we assume $q\bar{q}$ ($n\bar{n}$ or $s\bar{s}$) creation and annihilation to take place according to the empirically successful $^3P_0$ model [19], that is, with vacuum quantum numbers $J^{PC} = 0^{++}$. At first sight it may seem odd to couple $s\bar{s}$ states to pions, but the next-order diagram in the figure shows that the $K\bar{K}$ and $\eta\eta$ loops in the intermediate state will inevitably lead to a
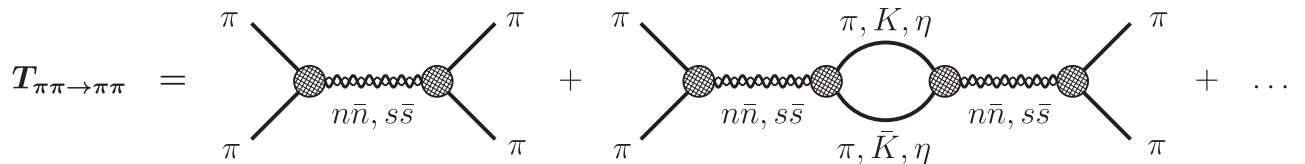


$$T_{\pi\pi \to \pi\pi} = \quad + \quad + \quad \cdots$$

FIG. 1. Graphical representation of the $\pi\pi \to \pi\pi$ element of the $3 \times 3$ $T$-matrix, with $\pi\pi$, $K\bar{K}$, and $\eta\eta$ loops between the $n\bar{n}$ and $s\bar{s}$ propagators in the intermediate state. The dots stand for all higher-order terms in the $s$-channel bubble sum.

mixing of the bare $n\bar{n}$ and $s\bar{s}$ states, thus allowing both mixed states to couple to $\pi\pi$. Clearly, the whole bubble sum can be easily summed up algebraically. In other words, since the effective interaction represented by the Born term in the figure is separable, just like similar diagrams with $K\bar{K}$ and/or $\eta\eta$ pairs in initial and/or final state, the complete three-channel $T$-matrix can be straightforwardly solved in closed form.

The full expression for the effective interaction, symbolized by the Born term for the $\pi\pi \to \pi\pi$ process in Fig. 1, reads explicitly (also see Ref. [18])

$$V_{ij}(p_i, p'_j; E) = \lambda^2 j_0^i(p_i a) \mathcal{R}_{ij}(E) j_0^j(p'_j a), \qquad (1)$$

$$\mathcal{R}_{ij}(E) = \sum_{\alpha=1}^{2} \sum_{n=0}^{\infty} \frac{g_{(\alpha,n)}^i g_{(\alpha,n)}^j}{E - E_n^{(\alpha)}}, \qquad (2)$$

where the RSE propagator $\mathcal{R}$ contains an infinite tower of bare $n\bar{n}$ and $s\bar{s}$ states with quantum numbers $J^{PC} = 0^{++}$ corresponding to the discrete scalar spectrum of an in principle arbitrary confining potential. Also, $E_n^{(\alpha)}$ is the energy level of the $n$th recurrence in the $\alpha$th $q\bar{q}$ channel, with $\alpha = 1$ referring to $n\bar{n}$ and $\alpha = 2$ to $s\bar{s}$, while $g_{(\alpha,n)}^i$ is the corresponding coupling to the $i$-th MM channel. Furthermore, in Eq. (1), $\lambda$ is the overall coupling constant for $^3P_0$ decay, and $j_0^i(p_i)$ and $p_i$ are the zeroth order ($L = 0$) spherical Bessel function and the (relativistically defined) off-energy-shell relative momentum in MM channel $i$, respectively. The spherical Bessel function originates in our sharp string-breaking picture of OZI-allowed decay at a certain radius $a$, being the Fourier transform of a spherical delta-shell at $r = a$. Such a picture is supported by LQCD simulations [20]. The channel couplings $g_{(\alpha,n)}^i$ in Eq. (2) are computed following the formalism developed in Ref. [21], namely from overlaps of harmonic-oscillator (HO) wave functions for the original $q\bar{q}$ pair, the created $^3P_0$ pair, and the two $q\bar{q}$ states corresponding to the outgoing two mesons. In most cases, this method produces the same couplings for ground-state mesons as the usual point-particle recoupling schemes of spin, isospin, and orbital angular momentum, but it also provides a clear prescription for excited mesons, with the additional advantage of always resulting in a finite number of nonvanishing couplings. Because of their fast decrease for increasing radial quantum number $n$, practical convergence of the infinite sum in Eq. (2) is achieved by truncating it after at most 20 terms. Moreover, the method guarantees rigorous flavor symmetry for all nonexotic mesons, including the $\sigma$ (see discussion and examples in Refs. [22–24]).

With the separable effective and energy-dependent MM potential in Eqs. (1) and (2), the $3 \times 3$ fully off-energy-shell $T$-matrix can be solved directly, yielding

$$T_{ij}(p_i, p'_j; E) = -2a\lambda^2 \sqrt{\mu_i p_i} j_0^i(p_i a)$$

$$\times \sum_{m=1}^{N} \mathcal{R}_{im} \{[\mathbb{1} - \Omega\mathcal{R}]^{-1}\}_{mj} j_0^j(p'_j a) \sqrt{\mu_j p'_j}, \qquad (3)$$

with the loop function

$$\Omega_{ij}(k_j) = -2ia\lambda^2 \mu_j k_j j_0^j(k_j a) h_0^{(1)j}(k_j a)\delta_{ij}, \qquad (4)$$

where $h_0^{(1)j}(k_j a)$ is the spherical Hankel function of the first kind, $k_j$ and $\mu_j$ are the on-shell relativistic relative momentum and reduced mass in MM channel $j$, respectively, and the matrix $\mathcal{R}(E)$ is given by Eq. (2). Note that no regularization is needed in this model to all orders, since the Bessel functions at the vertices make the meson loops finite. The manifestly analytic and unitary $S$-matrix is simply given by

$$\mathcal{S} = \mathbb{1} + 2i\hat{T}, \qquad (5)$$

where $\hat{T}$ is the fully on-energy-shell submatrix of $T$, restricted to the kinematically allowed MM channels just like $\mathcal{S}$. From Eqs. (1)–(5), the cotangent of the $S$-wave $\pi\pi$ phase shift can then be expressed as

$$\cot(\delta_{\pi\pi}^{(0)}) = i + \frac{\eta_{\pi\pi}^{(0)}}{\hat{T}_{\pi\pi\to\pi\pi} - i\frac{1-\eta_{\pi\pi}^{(0)}}{2}}, \qquad (6)$$

where $\eta_{\pi\pi}^{(0)}$ is the inelasticity in the $\pi\pi \to \pi\pi$ channel, with $\eta_{\pi\pi}^{(0)} = 1$ for $E < 2m_K$ and $|\mathcal{S}_{\pi\pi\to\pi\pi}|$ otherwise.

Before we now carry out a fit to the $S$-wave $\pi\pi$ phase shift, let us introduce one more phenomenological degree of freedom, namely the intrinsic mixing between the bare $n\bar{n}$ and $s\bar{s}$ states. It is true that the common $K\bar{K}$ and $\eta\eta$ channels, via $s\bar{s}$ and/or $n\bar{n}$ creation, inexorably lead to such a mixing beyond the Born approximation, but an additional mixing already at the quark level is perfectly possible, namely via two gluons. Since low-energy QCD does not allow to rigorously compute this mixing, we here introduce the corresponding angle $\Theta_S$ as a free fit parameter, just like in Ref. [18]. The other parameters to be varied in the fit are the overall coupling $\lambda$ and the decay radius $a$. The original model parameters we keep exactly equal to their values as fixed in Ref. [7] and then used in Ref. [8] as well as in all posterior model calculations, both in coordinate-space and momentum-space approaches. These fixed parameters are: the constituent quark masses $m_n = 406$ MeV and $m_s = 508$ MeV, besides the constant level splittings $2\omega = 380$ MeV and $\omega = 190$ MeV between radial and orbital excitations, respectively. The latter equidistant HO spectrum is clearly not a canonical one in meson spectroscopy, but its choice is immaterial for the present study, because
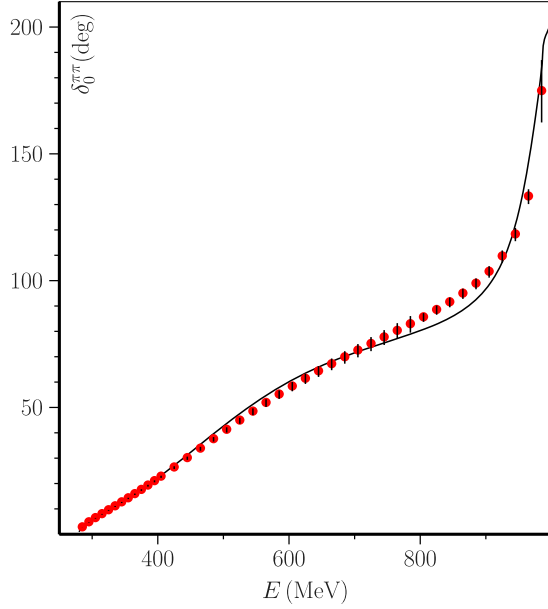
FIG. 2. Model fit to $S$-wave $\pi\pi$ phase shifts from Ref. [26].

the resulting lowest standard $n\bar{n}$ and $s\bar{s}$ states come out at about 1.3 GeV and 1.5 GeV, respectively, very close to the values found in mainstream quark models. For theoretical and empirical justifications of a mass-dependent HO potential, see Refs. [6,25]. The latter reference concerns a review paper that revisits many successful meson-spectroscopy applications of such a potential in the framework of unitarized quark models.

Now we are in a position to fit $\lambda$, $a$, and $\Theta_S$ to $S$-wave $\pi\pi$ phase shifts from threshold up to 1 GeV collected and compiled by D. V. Bugg [26] from various sources (also see Ref. [27]). The fitted parameter values are[1]

$$\lambda = 3.673, \quad a = 3.314\,\text{GeV}^{-1}, \quad \Theta_S = 7.515°. \quad (7)$$

These values of $\lambda$ and $a$ are close to those found in Ref. [18]. But note that the fitted $\Theta_S$ is much smaller here than in Ref. [18], which is plausible, as in the latter paper a much larger energy interval had to be accommodated. For the same reason, we now do not impose an explicit extra damping of closed channels like in Ref. [18]. Owing to this small value of $\Theta_S$, our bare $n\bar{n}$ and $s\bar{s}$ states are almost pure, with most of the mixing between the $\sigma$ and $f_0(980)$ resulting from the common $K\bar{K}$ and $\eta\eta$ channels. The result of the fit to the $\pi\pi$ phases is shown in Fig. 2. The quality of the fit is satisfactory, considering the mere three adjustable parameters. The kink in the model curve at about 990 MeV is due to the opening of the $K\bar{K}$ channel,

---

[1]Note that in Ref. [18] a wrong dimension of $\text{GeV}^{-1/2}$ was specified for $\lambda$. With $\lambda$ defined as in Eqs. (1)–(4), it is dimensionless.

which introduces an $S$-wave inelasticity in the $\pi\pi$ channel. Also note that the almost perfect fit at low energies is reflected in the obtained isoscalar $S$-wave $\pi\pi$ scattering length $a_0^0 = 0.211 m_\pi^{-1}$. Finally, we find the two isoscalar scalar resonance poles on the second Riemann sheet (in MeV) $\sigma(460 - i222)$ and $f_0(978 - i37.2)$.

## III. $\sigma(500)$ POLES AS A FUNCTION OF $m_\pi$

As already mentioned in the Introduction, Ref. [11] has studied the isoscalar scalar system in lattice simulations for two unphysical pion masses, viz. $m_\pi = 391$ MeV [10,11] and $m_\pi = 236$ MeV [10]. For the smaller pion mass, a resonance pole could be extracted resembling the $\sigma(500)$, albeit with a too large real part. However, this extraction is difficult and leads to widely scattered values for the real and imaginary part of the pole, depending on the employed parametrization [10]. Moreover, in order to extrapolate these results toward the physical pion mass, different methods may be used as well. In that spirit, we compute here $\sigma$ pole positions as a continuous function of $m_\pi$, leading to bound-state, virtual-state, and resonance trajectories, which we shall display next both in the complex energy and momentum planes.

The numerical technique I use to search for real or complex poles in the $\mathcal{S}$-matrix is by finding the zeroes in the modulus squared of the determinant of the matrix $\mathbb{1} - \Omega\mathcal{R}$ in Eq. (3), just like already done for the $\sigma(500)$ and $f_0(980)$ resonances above. This is easy by employing the Fortran-coded minimization package MINUIT of the CERN Program Library [28].

In Fig. 3 the resonance pole trajectory of the $\sigma(500)$ in the complex $E$ plane is shown for a pion mass ranging from its physical value to $m_\pi = 261.57$ MeV, where the pole reaches the real axis and splits into a pair of virtual-state poles, i.e., staying on the second Riemann sheet. Note that for $m_\pi > 231.21$ MeV we are dealing with a typical subthreshold $S$-wave resonance, just like in the case of making the resonance pole move to the real axis by increasing the overall coupling $\lambda$ (see Fig. 2 in Ref. [17]). What is quite remarkable is the enormous stability of the real part of the resonance pole, increasing by only about 3 MeV while the imaginary part runs from $-222$ MeV to zero. Figure 3 also indicates the resonance pole for the pion mass of 236 MeV employed in Ref. [10]. The equivalent pole trajectory in the complex $k$ plane is displayed in Fig. 4, where the mirror-image trajectory with $\mathcal{R}e(k) < 0$, required for unitarity [25], is not shown. The latter two poles meet on the negative imaginary $k$ axis for $m_\pi = 261.57$ MeV, indeed confirming that we are dealing now with virtual poles. This typical $S$-wave behavior of $\mathcal{S}$-matrix poles is further clarified by allowing $m_\pi$ to become even larger. So in Fig. 5 the real trajectories of bound-state and virtual-state poles are displayed by plotting the corresponding energies directly as a
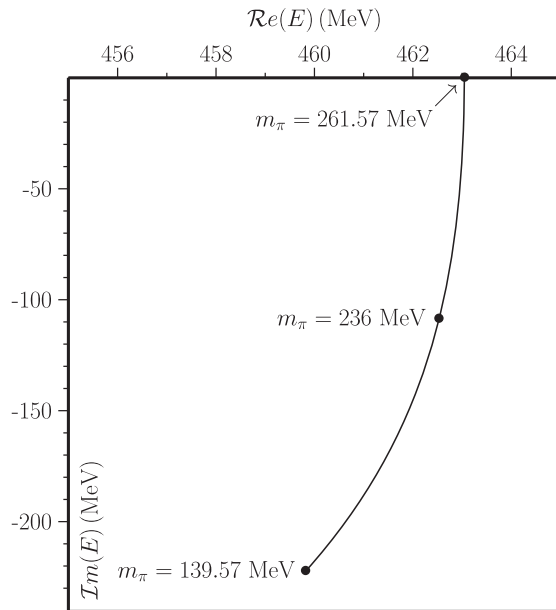
FIG. 3. Resonance pole trajectory of $\sigma(500)$ in the complex $E$ plane as a function of $m_\pi$.



FIG. 5. Bound-state and virtual-state pole trajectories of real $\sigma(500)$ energy as a function of $m_\pi$; green (upper section): bound state, blue (middle section): first virtual state, red (lower section): second virtual state.

double-valued function of $m_\pi$, up to $m_\pi = 500$ MeV. First of all, a $\sigma(500)$ bound state is found at $E = 710.3$ MeV for the pion mass of 391 MeV used in Refs. [10,11]. We also see that, for all values of $m_\pi > 261.57$ MeV, there are two real poles, i.e., one bound state plus one virtual state or two virtual states, the latter meeting at 261.57 MeV to transform into one resonance for smaller values of $m_\pi$. Also this behavior is qualitatively the same as that observed in the case of
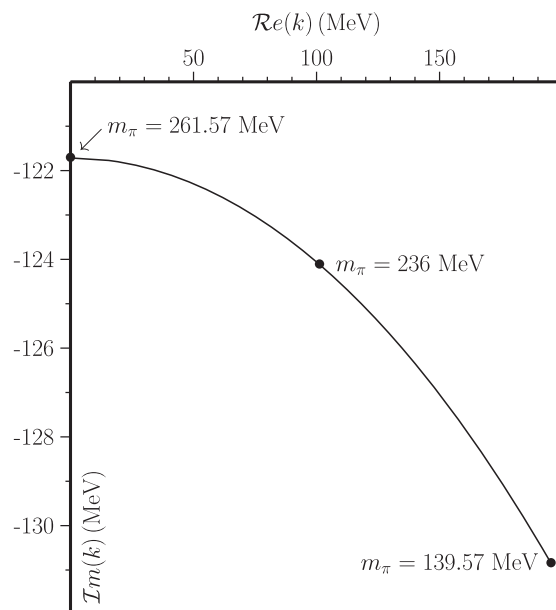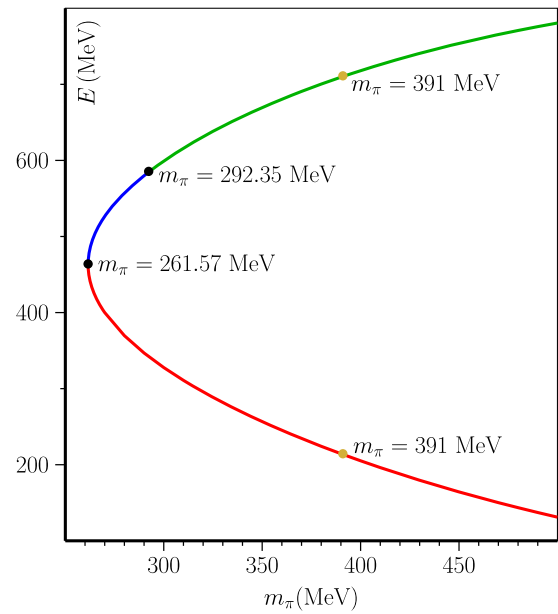
pole trajectories as a function of $\lambda$ [17,18]. Moreover, Fig. 5 shows that in the bound-state situation, there is only a very far-away virtual pole, contrary to the claim in Ref. [16], as argued in Ref. [17] as well. Finally, Fig. 6 displays the corresponding (imaginary) momentum trajectory of bound and virtual states.
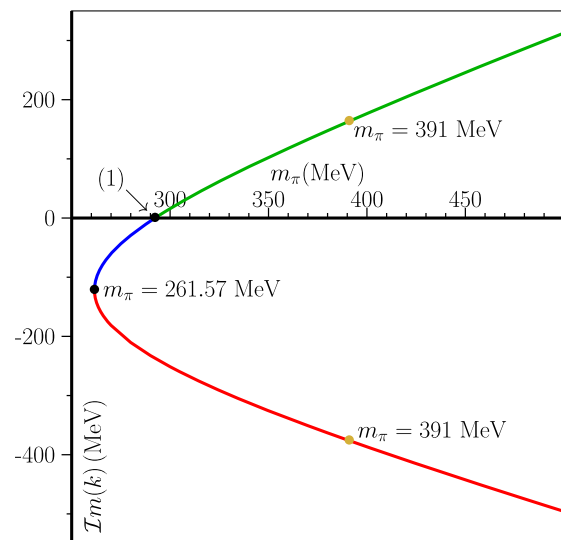


FIG. 4. Resonance pole trajectory of $\sigma(500)$ in the complex $k$ plane as a function of $m_\pi$, for $\mathcal{Re}(k) > 0$.



FIG. 6. Bound-state and virtual-state pole trajectories of imaginary $\sigma(500)$ momentum as a function of $m_\pi$; green (upper section): bound state, blue (middle section): first virtual state, red (lower section): second virtual state. Point (1): $m_\pi = 292.35$ MeV.

## IV. DISCUSSION AND CONCLUSIONS

Before comparing the above model results to recent LQCD predictions, let me mention two related works from about a decade ago. In Ref. [29], it was shown that the trajectories of poles as a function of some strength parameter and coupling to continuum $P$-waves or higher are qualitatively the same, irrespective of the employed dynamics. On the other hand, in the case of $S$-wave pole trajectories it was suggested that important information on the internal structure of a resonance can be revealed. As for Ref. [30], the authors made use of unitary chiral perturbation theory to study the pion-mass dependence of the size of the $\sigma(500)$, then on the verge of being renamed from $f_0(600)$ to $f_0(500)$ [2]. They concluded that for a large pion mass, of the order of 400 MeV, the picture of a molecular-type, spread-out $\pi\pi$ state appears to be suitable. This would indeed resemble somewhat the relatively small $\pi\pi$ binding for $m_\pi = 391$ MeV, as later found on the lattice in Refs. [10,11,14,15]. However, for the physical pion mass they obtained a small $\sigma(500)$ size suggesting a compact object, for which the authors considered a four-quark picture more appropriate. I disagree with the latter assessment, based on the above model results, as well as the referred lattice computations, in which no four-quark interpolators were employed.

We will now compare our continuous $\sigma(500)$ trajectories with the discrete $\sigma$ lattice pole positions for $m_\pi =$ 391 MeV [10,11] and $m_\pi = 236$ MeV [10]. Starting with the bound-state case, we recall the model prediction 710.3 MeV, whereas the lattice yielded 758(4) MeV [10] and 745(5) MeV [11], for $m_\pi = 391$ MeV. This discrepancy is probably due to a difference in the handling of the $K\bar{K}$ and $\eta\eta$ channels. First of all, in Ref. [11] Kaon and $\eta$ masses were employed of 549 MeV and 587 MeV, respectively, instead of the physical ones, as a result of the chosen light and strange quark masses. Although such an increased $K$ mass was not mentioned in Ref. [10], probably the same or a similar value was taken. The small difference in binding energy of 13 MeV between the two simulations in Refs. [10,11] appears to be indeed due to the inclusion of the $\eta\eta$ channel in Ref. [11], by providing some extra attraction owing to the latter kinematically closed channel. If we also increase the Kaon and $\eta$ masses in the model as in Ref. [11], the $\sigma$ mass comes out at 718 MeV. Now we should recall that, in the more general model of Ref. [18], a phenomenological damping of closed channels was introduced in order to reduce their influence far underneath the thresholds, which becomes necessary when simultaneously fitting data over a very wide energy range. A similar suppression of closed channels was successfully used in Ref. [27], dealing with the complete scalar nonet. As mentioned in Ref. [17], a $\sigma$ bound state of 760 MeV is found in the full model of Ref. [18], for a pion mass of 391 MeV. If we here use the same subthreshold suppression of the $K\bar{K}$ and $\eta\eta$ channels as in Ref. [18], the bound state comes out at 752 MeV.

In the very recent LQCD paper of Ref. [14], further information on the quark-mass dependence was obtained by carrying out computations of the $\sigma$ pole at two intermediate pion masses, viz. $m_\pi = 283$ MeV and $m_\pi = 330$ MeV. The authors concluded that the $\sigma$ undergoes a transition from being a bound state to a virtual bound state somewhere between these two values of the pion mass. This is in agreement with the model results displayed in Figs. 5 and 6, with the transition from bound state to virtual state occurring at $m_\pi = 292.35$ MeV. Also the typical $S$-wave behavior of the $\sigma$ pole near threshold as observed in Ref. [14] is in conformity with our findings above. Still regarding a real $\sigma$ pole, the conclusion in the other very recent LQCD paper [15] that the $\sigma$ appears to pass through a narrow virtual-state region upon transitioning from a bound state to a (subthreshold) resonance is qualitatively what one also observes in Figs. 5 and 6.

Finally we compare the model's $\sigma$-pole resonance trajectories in Figs. 3 and 4 with the LQCD results in Refs. [10,15]. As mentioned before, the former lattice computation for $m_\pi = 236$ MeV resulted in complex pole positions strongly varying with the employed parametrizations of the computed real amplitudes, such as $K$-matrix, relativistic Breit-Wigner, and other ansatzes, with or without an Adler zero. From Fig. 5 in Ref. [10], I extract an energy range of about 590–760 MeV for the poles' real parts and approximately 280–460 MeV for the widths, i.e., twice the modulus of the imaginary parts. On top of that are the quite large error bars, up to roughly $\pm 80$ MeV in one case. So even accounting for the uncertainties in the various resonance pole positions, they all lie well above the $\pi\pi$ threshold at 472 MeV. In this respect, it is interesting to note that two of the lowest mass predictions, albeit still above 500 MeV, concern parametrizations with an Adler zero. Namely, in Ref. [31] a relativistic Breit-Wigner form with an explicit Adler zero in the $s$-dependent width was used to fit $S$-wave $\pi\pi$ phase shifts, which in combination with other data yielded a $\sigma(500)$ pole position with real part $(533 \pm 25)$ MeV. Also, in Ref. [18] a very simple yet unitary Breit-Wigner form was shown to overestimate the resonance mass. In comparison, the present unitary and analytic model predicts a very small interval 460–463 MeV for the real part of the $\sigma(500)$ pole while covering a wide range of pion masses, including $m_\pi = 236$ MeV. Nevertheless, a significant LQCD improvement was accomplished in Ref. [15] by imposing constraints through dispersive approaches, with the corresponding resonance pole positions displayed in Fig. 3 of that paper. Note that the pion mass in this case was taken at 239 MeV, which owing to an improved extraction [14] corresponds to $m_\pi = 236$ MeV used in Ref. [10]. From the figure I now extract the ranges 498–586 MeV for the real parts and

394–506 MeV for the widths, with the largest error in the real part being $\pm 82$ MeV. These values allow for a possible subthreshold $\sigma$ resonance at $m_\pi = 239$ MeV for two of the employed dispersive methods, as found in the present model (see Figs. 3 and 4). The largest discrepancy between lattice and model we observe for the width of the $\sigma$, which is at least 350 MeV in Ref. [15] and only about 220 MeV in the model for $m_\pi = 236$ MeV. So I conclude that it would be worthwhile to compute the $\sigma$ resonance on the lattice for some pion masses between 239 MeV and 283 MeV, in order to see how the width can get down from about 400–500 MeV to zero very fast over a relatively small range of pion masses, namely of the order of 40–50 MeV.

[1] R. L. Workman *et al.* (Particle Data Group), Prog. Theor. Exp. Phys. **2022**, 083C01 (2022).

[2] G. Rupp and E. van Beveren, Acta Phys. Pol. B Suppl. **11**, 455 (2018).

[3] R. L. Jaffe, Phys. Rev. D **15**, 267 (1977).

[4] G. Rupp and E. van Beveren, Chin. Phys. C **41**, 053104 (2017).

[5] C. Dullemond, T. A. Rijken, E. van Beveren, and G. Rupp, On the influence of hadronic decay on the properties of hadrons, *6th Warsaw Symposium on Elementary Particle Physics, 1983* (Kazimierz, Poland, 1983), Nijmegen report THEF-NYM-83.09.

[6] E. van Beveren, T. A. Rijken, C. Dullemond, and G. Rupp, Lect. Notes Phys. **211**, 331 (1984).

[7] E. van Beveren, G. Rupp, T. A. Rijken, and C. Dullemond, Phys. Rev. D **27**, 1527 (1983).

[8] E. van Beveren, T. A. Rijken, K. Metzger, C. Dullemond, G. Rupp, and J. E. Ribeiro, Z. Phys. C **30**, 615 (1986).

[9] R. A. Briceno, J. J. Dudek, and R. D. Young, Rev. Mod. Phys. **90**, 025001 (2018).

[10] R. A. Briceno, J. J. Dudek, R. G. Edwards, and D. J. Wilson, Phys. Rev. Lett. **118**, 022002 (2017).

[11] R. A. Briceno, J. J. Dudek, R. G. Edwards, and D. J. Wilson, Phys. Rev. D **97**, 054513 (2018).

[12] E. van Beveren and G. Rupp, Int. J. Theor. Phys. Group Theory Nonlinear Opt. **11**, 179 (2006), https://arxiv.org/abs/hep-ph/0304105.

[13] E. van Beveren and G. Rupp, Ann. Phys. (Amsterdam) **324**, 1620 (2009).

[14] A. Rodas, J. J. Dudek, and R. G. Edwards (Hadron Spectrum Collaboration), Phys. Rev. D **108**, 034513 (2023).

[15] A. Rodas, J. J. Dudek, and R. G. Edwards, arXiv:2304.03762.

[16] X. L. Gao, Z. H. Guo, Z. Xiao, and Z. Y. Zhou, Phys. Rev. D **105**, 094002 (2022).

[17] E. van Beveren and G. Rupp, Phys. Rev. D **107**, 058501 (2023).

[18] E. van Beveren and G. Rupp, *Gribov-90 Memorial Volume* (World Scientific, Singapore, 2021), pp. 201–216, 10.1142/9789811238406_0020.

[19] L. Micu, Nucl. Phys. **B10**, 521 (1969).

[20] G. S. Bali, H. Neff, T. Düssel, T. Lippert, and Klaus Schilling (SESAM Collaboration), Phys. Rev. D **71**, 114513 (2005).

[21] E. van Beveren, Z. Phys. C **17**, 135 (1983).

[22] E. van Beveren and G. Rupp, Eur. Phys. J. C **10**, 469 (1999).

[23] E. van Beveren and G. Rupp, Eur. Phys. J. C **11**, 717 (1999).

[24] E. van Beveren and G. Rupp, Phys. Lett. B **454**, 165 (1999).

[25] E. van Beveren and G. Rupp, Prog. Part. Nucl. Phys. **117**, 103845 (2021).

[26] D. V. Bugg (private communication).

[27] E. van Beveren, D. V. Bugg, F. Kleefeld, and G. Rupp, Phys. Lett. B **641**, 265 (2006).

[28] https://root.cern.ch/download/minuit.pdf.

[29] C. Hanhart, J. R. Pelaez, and G. Rios, Phys. Lett. B **739**, 375 (2014).

[30] M. Albaladejo and J. A. Oller, Phys. Rev. D **86**, 034003 (2012).

[31] D. V. Bugg, Phys. Lett. B **572**, 1 (2003); **595**, 556(E) (2004).